Analysis of Syngas Production from Biogas via the Tri-Reforming Process

Rei-Yu Chein * and Wen-Hwai Hsu

Department of Mechanical Engineering, National Chung Hsing University, Taichung City 40227, Taiwan; dawnxcirno@gmail.com
* Correspondence: rychein@dragon.nchu.edu.tw; Tel.: +886-4-2284-0433

check for updates

Abstract: The tri-reforming process was employed for syngas production from biogas at elevated pressures in this study. In the tri-reforming process, air and water were added simultaneously as reactants in addition to the main biogas components. The effects of various operating parameters such as pressure, temperature and reactant composition on the reaction performance were studied numerically. From the simulated results, it was found that methane and carbon dioxide conversions can be enhanced and a higher hydrogen/carbon monoxide ratio can be obtained by increasing the amount of air. However, a decreased hydrogen yield could result due to the reverse water–gas shift reaction. A higher level of methane conversion and hydrogen/carbon monoxide ratio can be obtained with increased water addition. However, negative carbon dioxide conversion could result due to the water–gas shift and reverse carbon dioxide methanation reactions. The dry reforming reaction resulting in positive carbon dioxide conversion can only be found at a high reaction temperature. For all cases studied, low or negative carbon dioxide conversion was found because of carbon dioxide production from methane oxidation, water–gas shift, and reverse carbon dioxide methanation reactions. It was found that carbon dioxide conversion can be enhanced in the tri-reforming process by a small amount of added water. It was also found that first-law efficiency increased with increased reaction temperature because of higher hydrogen and carbon monoxide yields. Second-law efficiency was found to decrease with increased temperature because of higher exergy destruction due to a more complete chemical reaction at high temperatures.

Keywords: biogas; tri-reforming process; syngas; methane and carbon dioxide conversion; hydrogen/carbon monoxide ratio; first-law/second-law efficiency

1. Introduction

The efficient production of syngas (a mixture of hydrogen and carbon monoxide) is gaining significant attention worldwide as it is a versatile feedstock that can be used to produce a variety of fuels and chemicals, such as methanol, Fischer–Tropsch fuels, H_2, and dimethyl ether (DME) [1]. Using CH_4 as the primary material, syngas can be produced from steam reforming (SR), partial oxidation (POX), autothermal reforming (ATR), and dry reforming (DR). The tri-reforming (TR) process for syngas production from CH_4 has received growing attention because of its technical simplicity and flexible operation [2–5]. In the TR process, the syngas is produced by combining SR, DR, and POX in a single step. The TR process was proposed originally for syngas production from power plant flue gas [6,7]. There are several advantages for syngas production from the TR process. As CO_2 is one of the reactants, there is no need for CO_2 separation from the flue gas [6,7]. The H_2/CO ratio in syngas can be altered by adjusting the relative amounts of the reactants. In addition, the presence of H_2O and O_2 in the feedstock helps to mitigate carbon deposition, and catalyst deactivation can be prevented [8,9].

As fossil energy resources reduce sharply and environmental pollution becomes more serious, searching for new materials for syngas production plays an important role in future energy development [10–12]. Biogas is receiving much attention because of its considerable economic and environmental benefits [13]. The biogas composition is related to the starting substrate, but is basically composed of CH_4 and CO_2 with the volume ratio of 2 [14–16]. Both CH_4 and CO_2 are regarded as major greenhouse gases (GHGs), which pose a serious threat to the global climate and environment. Using biogas for syngas production, both CH_4 and CO_2 emissions into the atmosphere can be reduced. Because of its potential for reducing global warming, further understanding of syngas production from biogas is essential. Moreover, syngas can also be used for H_2 production. In this case, H_2 can be enriched via the water–gas shift reaction using syngas and H_2O as feedstock. Among the various alternative energy forms, hydrogen is considered an important energy carrier in the future [17]. It is also an important raw material in the chemical industry and can be used as a fuel in fuel cells to produce electrical energy. For reasons of sustainability, the use of renewable fuel sources such as biogas or biomass for hydrogen production has received considerable attention [18–20].

Several studies have reported on syngas production from biogas via the TR process experimentally. In the study of Vita et al. [21], tri-reforming simulated biogas over a Ni/ceria based catalysts was carried out and the H_2O/CH_4 and O_2/CH_4 molar ratios, reaction temperature, and nickel content effects on the catalyst's performance were studied. They found that the H_2/CO ratio could be flexibly adjusted using added amounts of oxygen and steam in order to meet the requirements of downstream processes. In the study of Lau et al. [22], biogas was used as the fuel source in dry reforming and combined dry/oxidative reforming reactions. The gas stream temperature and reactor space velocity effects were examined experimentally. Their results indicated that an increase in the O_2/CH_4 ratio at low temperature promotes hydrogen production. In dry/oxidative reforming, they found that biogas dry reforming is dominant and the overall reaction is net endothermic when the reaction temperature is higher than 600 °C. In the study of Zhu et al. [23], biogas reforming with added O_2 through a spark-shade plasma was conducted under an O_2/CH_4 ratio of 0.60 and CO_2/CH_4 ratios ranging from 0.17 to 1.00. Their results indicated that O_2 and CH_4 conversions decreased when the CO_2/CH_4 ratio was increased. They also reported that the partial oxidation of methane contributed mostly to CH_4 conversion and the reverse water–gas shift (WGS) reaction dominated in CO_2 conversion.

In addition to experimental work, several numerical TR process models using biogas as the feedstock have also been reported in the literature. In the study of Corigliano and Fragiacomo [24], biogas dry reforming analysis under various operating conditions was carried out using a numerical model. The CO_2/CH_4 ratio, pressure and temperature effects on reaction performance were reported. In the study of Hernández and Martín [25], a process based on mass and energy balances, chemical and phase equilibria, and rules of thumb was developed to optimize the production of methanol using biogas as the raw material. Based on the production cost and carbon footprint, the optimized CH_4/CO_2 ratio contained in the biogas was found. In the study of Hajjaji et al. [26], a H_2 production system via biogas reforming was investigated using life-cycle assessment (LCA). They found that the total GHG emissions from the system were about half of the life-cycle GHG of conventional H_2 production systems via steam methane reforming. In the study of Zhang et al. [27], the effects of various factors including reaction temperature, reactor pressure and CH_4 flow rate on the syngas compositions obtained from the TR process were investigated numerically. An optimum operating condition for syngas production with a target ratio and maximized CO_2 conversion were obtained.

In this work, the TR process is employed for syngas production using biogas as the feedstock. The effects of various operating conditions such as pressure, temperature, biogas composition, air addition, and H_2O additions are investigated. The novelty of this paper is the focus on CO_2 conversion in the TR process, which is seldom reported in the literature. Air is used as the added reactant in this study instead of pure oxygen in the conventional TR process.

2. Modeling

2.1. Chemical Reaction

The following reactions are coupled and carried out in a single reactor in the TR porcess:

Steam reforming (SR):

$$CH_4 + H_2O \leftrightarrow CO + 3H_2, \ \Delta H^0_{298K} = +206 \text{ kJ/mole} \tag{1}$$

Dry reforming (DR):

$$CH_4 + CO_2 \leftrightarrow 2CO + 2H_2, \ \Delta H^0_{298K} = +247 \text{ kJ/mole} \tag{2}$$

Partial oxidation (POX):

$$CH_4 + 0.5O_2 \leftrightarrow CO + 2H_2, \ \Delta H^0_{298K} = -36 \text{ kJ/mole} \tag{3}$$
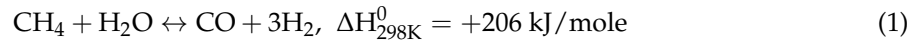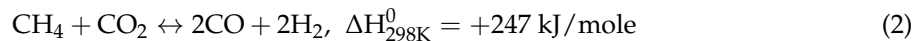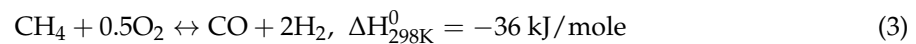
As shown in Equations (1)–(3), the TR process combines the endothermic SR and DR reactions and the exothermic POX reaction. The heat released from POX is used as the heat supply for SR and DR and makes the TR process energy efficient [28]. As noted by Cho et al. [29], the chemical reactions involved in the TR process can be alternatively described using Equation (1) along with the following reactions:

Reverse CO_2 methanation (RCM):

$$CH_4 + 2H_2O \leftrightarrow CO_2 + 4H_2, \ \Delta H^0_{298K} = +165 \text{ kJ/mole} \tag{4}$$

Water-gas shift (WGS):

$$CO + H_2O \leftrightarrow CO_2 + H_2, \ \Delta H^0_{298K} = -41 \text{ kJ/mole} \tag{5}$$
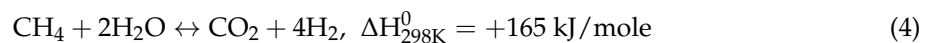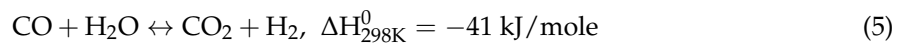
Complete oxidation of methane (COM):

$$CH_4 + 2O_2 \leftrightarrow CO_2 + 2H_2O, \ \Delta H^0_{298K} = -803 \text{ kJ/mole} \tag{6}$$
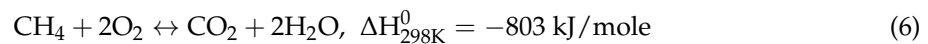
Note that with the chemical reactions described in Equations (1) and (4)–(6), the TR process becomes the well-known catalytic partial oxidation of methane (CPOM). In the literature, there are many studies devoted to the analysis of kinetic mechanisms for CPOM [30,31]. Similar to other reforming process of CH_4, many reactions are likely to occur in the TR process. In addition to the study of Cho et al. [29], studies of De Groote and Froment [32], Scognamiglio et al. [33], Chan and Wang [34], and Izquierdo et al. [35] also reported that the reaction mechanism of CPOM is indirect in which the process can be described by combining reactions of methane oxidation, methane–steam reforming, and water–gas shift. According to these studies, reactions such as CO oxidation, H_2 oxidation, and the Boudouard reaction were not included.

Equations (1), (4) and (5) are the reactions involved in the conventional SR reaction. In this study, syngas under high pressure is of interest for further fuel synthesis. The kinetic model for the SR reaction over a nickel catalyst given by Xu and Froment [36] is adopted,

SR:

$$r_1 = \frac{k_1}{p_{H_2}^{2.5}} \left[p_{CH_4} p_{H_2O} - \frac{p_{H_2}^3 p_{CO}}{K_{eq,1}} \right] / DEN^2 \tag{7}$$

WGS:

$$r_2 = \frac{k_2}{p_{H_2}} \left[p_{CO} p_{H_2O} - \frac{p_{H_2} p_{CO_2}}{K_{eq,2}} \right] / DEN^2 \tag{8}$$

RCM:

$$r_3 = \frac{k_3}{p_{H_2}^{3.5}}\left[p_{CH_4}p_{H_2O}^2 - \frac{p_{H_2}^4 p_{CO_2}}{K_{eq,3}}\right]/DEN^2 \tag{9}$$

$$DEN = 1 + K_{CH_4}p_{CH_4} + K_{CO}p_{CO} + K_{H_2}p_{H_2} + \frac{K_{H_2O}p_{H_2O}}{p_{H_2}} \tag{10}$$

For COM, the kinetic model of Trimm and Lam [37] is adopted in this study,

COM:

$$r_4 = \frac{k_{4a}p_{CH_4}p_{O_2}}{\left(1 + K_{CH_4}^C p_{CH_4} + K_{O_2}^C p_{O_2}\right)^2} + \frac{k_{4b}p_{CH_4}p_{O_2}}{\left(1 + K_{CH_4}^C p_{CH_4} + K_{O_2}^C p_{O_2}\right)} \tag{11}$$

Equation (11) was derived over Pt-based catalyst support, while the model adsorption parameters are adjusted for a Ni-based catalyst [38]. In Equations (7)–(11), r_i is the reaction rate for SR (i = 1), WGS (i = 2), RCM (i = 3), and COM (i = 4); $K_{eq,i}$ and k_i are the chemical equilibrium constant and rate constant for reaction i (i = 1,2,3,4); p_j (j = CH_4, CO_2, H_2O, H_2, and CO) is the partial pressure of species j; and K_j and K_j^C are the adsorption constants of species j. All of these kinetic parameters are given in the Arrhenius function type and are functions of temperature, and can be found in the literature [36,37]. It is noted that catalyst deactivation due to the thermal effect and carbon deposition is neglected in this study [39]. For a reforming reaction involving CH_4, carbon formation is inevitable. The carbon deposition on the catalyst surface is one of the reasons that causes catalyst deactivation. In the tri-reforming process, the appearances of O_2 and H_2O may suppress carbon formation [40,41]. Therefore, catalyst deactivation due to carbon deposition on the catalyst surface is neglected in this study.

2.2. Process Simulation

In this study, Aspen Plus (v.10) is employed to carry out the TR process using biogas as the feedstock. The flow process is depicted in Figure 1. The simulation is performed for a steady state. The biogas stream is assumed to be purely composed of CH_4 and CO_2 with the designated molar ratio. The air stream is composed of 21% O_2, 78% N_2, and 1% H_2. The purpose of H_2 addition is to avoid the singularity in chemical reaction rate computation. A 1% H_2 addition is determined through sensitivity analysis [42,43]. In order to produce high-pressure syngas for future use in fuel synthesis, two compressors (COM-1 and COM-2) are used to increase the biogas and air pressures. In the H_2O stream, a pump is used to increase the water pressure and it is then superheated in a boiler with heat supplied from the high-temperature product stream. After mixing in a mixer, the reactant mixture (TRI) is heated to a certain temperature before entering the insulated Rplug reactor (TR). The gas mixture from the reactor (TRO) is sent to the boiler where the heat is recovered for superheating the water. The TR process performance is characterized using the following dimensionless groups,

CH_4 and CO_2 conversions:

$$X_i = \frac{n_{i,in} - n_{i,out}}{n_{i,in}} \times 100\%, \ i = CH_4, CO_2 \tag{12}$$

H_2 yield:

$$Y_{H_2} = \frac{n_{H_2,out} - n_{H_2,in}}{n_{CH_4,in}} \tag{13}$$

CO yield:

$$Y_{CO} = \frac{n_{CO,out} - n_{CO,in}}{n_{CH_4,\ in}} \tag{14}$$

H_2/CO ratio:

$$H_2/CO = \frac{Y_{H_2}}{Y_{CO}} \tag{15}$$

where $n_{i,in}$ is the molar flow rate of the i-th species supplied to the process; and $n_{i,out}$ is the molar flow rate of the i-th species at reactor outlet. Based on these definitions, CH_4 conversion is the ratio of the CH_4 consumption rate to the fed CH_4 flow rate at the reactor inlet. Similarly, CO_2 conversion is the ratio of the CO_2 consumption rate to the fed CO_2 flow rate at the reactor inlet. The H_2 and CO yields are defined as the net increased amounts of H_2 and CO from the reaction per fed CH_4 flow rate. The H_2/CO ratio is defined as the ratio of H_2 yield to CO yield. Note that all these variables are dimensionless.
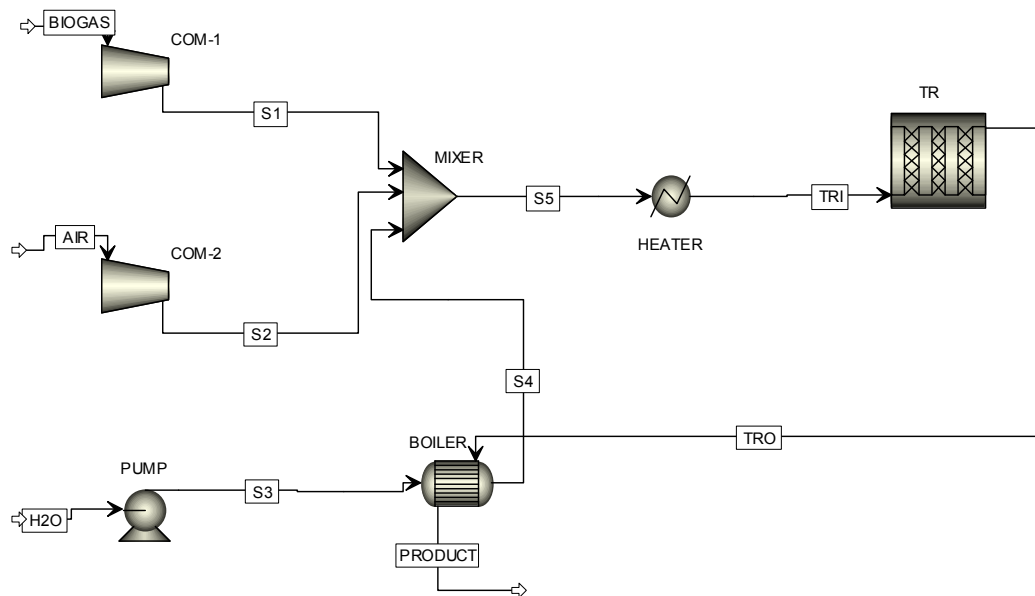
Figure 1. Tri-reform process for syngas production using biogas as feedstock.

In addition to the reactant conversion and product yield, energy and exergy analyses based on the resulting product stream flowing out of the TR reactor are also carried out. For the chemical reaction, there are several ways to define the first- and second-law efficiencies [44,45]. Since the objective of the TR process is to convert biogas into syngas, and noting that CO_2 has zero low heating value (LHV), the first-law efficiency is then defined as,

$$\eta_I = \frac{n_{CO,out}LHV_{CO} + n_{H_2,out}LHV_{H_2}}{n_{CH_4,in}LHV_{CH_4} + W_{comp} + W_{pump} + Q_{heat}} \times 100\% \tag{16}$$

where W_i (i = comp, pump) and Q_{heat} are the input work and heat input, respectively. The main heat input occurs at the heater at which the mixed reactant is heated to a certain inlet temperature. The exergetic analysis is carried out by considering three exergy transfers:

Exergy due to work:

$$Ex_W = W_{comp} + W_{pump} \tag{17}$$

Exergy due to heat transfer:

$$Ex_Q = Q_{heat}(1 - \frac{T_0}{T}) \tag{18}$$

Exergy due to mass flow:

$$Ex_{f,i} = N_i\{[(h - h_0) - T_0(s - s_0)] + \sum x_k e_k^{CH} + RT_0 \sum x_k \ln x_k\} \tag{19}$$

In these equations, the subscript 0 denotes the reference state (25 °C and 1 atm). The exergy due to mass flow is contributed by physical exergy, chemical exergy and mixing exergy as shown on the

right-hand side of Equation (19). For second-law efficiency, this is generally defined as the ratio of exergy recovered to the exergy supplied,

$$\eta_{II} = \frac{Ex_{out}}{Ex_{in}} \times 100\%$$

(20)

where Ex_{in} and Ex_{out} are the exergies supplied to and recovered from the system, respectively. Based on Figure 1, Ex_{in} and Ex_{out} are expressed as,

$$Ex_{in} = Ex_{biogas} + Ex_{air} + Ex_{H_2O} + Ex_Q + Ex_W, \; Ex_{out} = Ex_{product}$$

(21)

3. Results and Discussion

The TR process using biogas as the feedstock is similar to the tri-reforming of methane (TRM). The only difference is the CH_4 and CO_2 composition. We developed this work from our previous study [46] and focused on using biogas as the feedstock. To verify the correctness of the model built in Aspen Plus, the TRM using the reactor geometry and reactant composition reported in the studies of Chein et al. [46] and Arab Aboosadi et al. [47] was carried out using the built model in Aspen Plus. Figure 2 shows the comparison between the temperature and gas species distributions predicted from a two-dimensional model [46] and from a model built in Aspen Plus. As shown in Figure 2, the agreements for both temperature distribution shown in Figure 2a and species mole fractions shown in Figure 2b are quite good at the reactor downstream. The discrepancies in the region near the reactor inlet zone is believed due to the difference between one- and two-dimensional modeling. Since the TR process performance is evaluated using results at the reactor outlet, good agreement between one- and two-dimensional results is expected. In addition to the comparisons between numerical models, experimental verification of the numerical model was given in our previous study [46]. Also note that O_2 is consumed rapidly as it enters the reactor shown in Figure 2b. That is, there will be no O_2 available for oxidation of CO or H_2 in the downstream of the reactor.
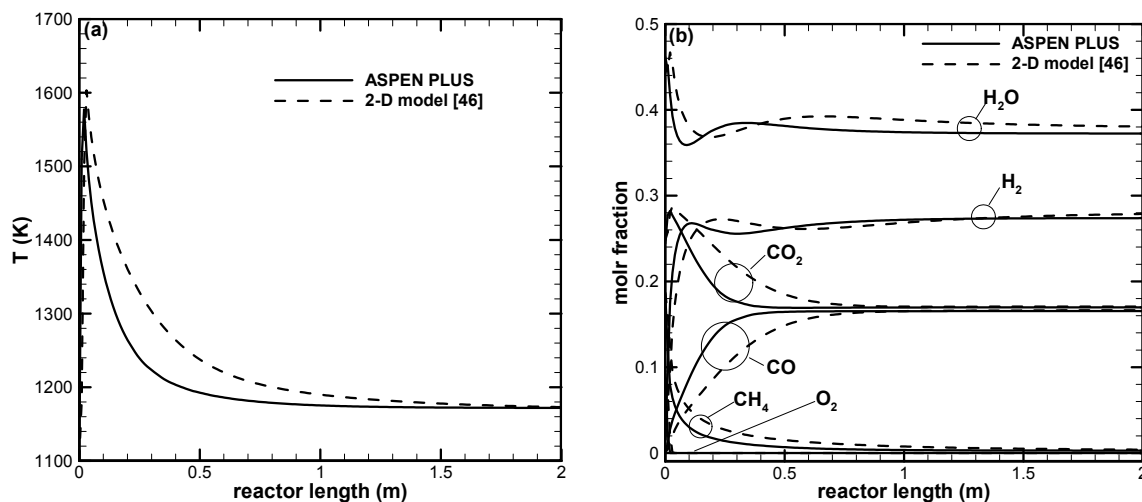
Figure 2. Comparison of results predicted from Aspen Plus and two-dimensional model [46] using the optimized reactant composition reported by Arab Aboosadi et al. [47]. T_{in} = 1100 K, p = 20 atm, and reactant composition $CH_4/CO_2/H_2O/O_2$ = 1/1.3/2.46/0.47. (**a**) Temperature and (**b**) species mole fraction variations along the reactor center line.

Based on the comparisons discussed above, the model built in Aspen Plus can be correctly extended to the TR process using biogas as the feedstock. The base operating conditions are listed in Table 1. The parameters listed in Table 1 are adopted from our previous study except for the

feedstock composition and total volumetric flow rate [46]. The molar ratio of the reactants are chosen as CH_4:CO_2:Air:H_2O = 1:0.5:2:1 and the volume flow rate is fixed as 0.0723 L/min. As compared with the previous study [46], a higher volume flow is used in this study because of the presence of N_2 in the air. For economy, air is added instead of pure oxygen. The advantage of this is to avoid the cost of oxygen separation from air, but this obviously results in increased reactor volume. In the following, the TR process performance is examined using reactant inlet temperature T_{in} as the primary parameter. The effects of various pressures, catalyst weight/volume flow rate (W/F) ratios, CO_2/CH_4 ratio in biogas, amounts of air and H_2O on TR process performance are discussed.

Table 1. Reactor geometry and base operation conditions [46,47].

Parameter	Value
Reactor length, L	2 m
Reactor diameter, d(=2R_b)	10 mm
Inlet pressure, p_{in}	20 atm
Inlet temperature, T_{in}	300~1000 °C
Reactant flow rate, F	0.0723 L min^{-1}
Molar ratio of biogas CH_4:CO_2:Air:H_2O	1:0.5:2:1
Catalyst	Ni/Al_2O_3
Catalyst size, d_p	0.42 mm
Catalyst weight, W	0.25 g
W/F ratio	0.0576 ghL^{-1}
Heat-transfer condition	Adiabatic

Figure 3 shows the TR process performance using the base operations listed in Table 1. In Figure 3a the temperature variation along the reactor length for T_{in} = 900 °C is shown. Due to the methane oxidation reaction, the maximum temperature occurs in the near entrance region. The energy produced from methane oxidation is used for steam reforming and dry reforming in the reactor downstream. This causes the temperature to decrease along the reactor length. The CH_4 and CO_2 conversions are shown in Figure 3b. The abrupt increase in CH_4 conversion occurs at T_{in} = 550 °C. This indicates that T_{in} should be higher than 550 °C in order to activate the catalyst. With temperature higher than 550 °C, CH_4 conversion increases gradually with increased T_{in}. In Figure 3b, negative CO_2 conversion results for the low T_{in} regime. From the TR process chemical reactions, CO_2 is produced by the methane oxidation and WGS reactions and consumed by the dry reforming reaction. For low T_{in}, the WGS reaction is dominated and CO_2 consumption by DR is low. This results in negative CO_2 conversion. However, positive CO_2 conversion can result when T_{in} becomes higher than 700 °C, indicating that DR is active. DR contributes to increase the H_2 and CO yield in the high T_{in} regime. Figure 3b also indicates that a complex interaction between CO_2 consumption and production reactions occurs for T_{in} in the 500~600 °C range. The conversions of CH_4 and CO_2 from an equilibrium TR process obtained from an Aspen Plus simulation are also shown in Figure 3b using the parameters listed in Table 1. Since the results from the equilibrium process can be regarded as the theoretical limit of the reaction, it can be seen that CH_4 conversion from the catalytic reaction is lower than that from the equilibrium reaction. Due to more CO_2 production, lower CO_2 conversion results from the equilibrium reaction. For T_{in} higher than 800 °C, CO_2 conversion from the equilibrium reaction is higher than that from the catalytic reaction. From Figure 3c, the H_2 yield, CO yield and H_2/CO ratio are shown. It can be seen that when T_{in} is lower than 500 °C, the H_2 and CO yields are very low due to inactive catalytic reactions at low temperatures. In this low T_{in} regime, CO yield is much lower than H_2 yield and results in a high H_2/CO ratio. As T_{in} is higher than 550 °C, the H_2/CO ratio decreases with T_{in} slowly with a value close to 2. The decrease in H_2/CO with T_{in} is due to increased CO production from the DR reaction while H_2 decreases due to the reverse WGS reaction. In Figure 3d, the H_2 yield, CO yield, and H_2/CO ratio from the equilibrium TR process are also shown. As with conversions of CH_4 and CO_2 shown in Figure 3b, both yields of H_2 and CO from the catalytic reaction are lower than

the equilibrium reaction. At high temperature, the H_2/CO ratio from both equilibrium and catalytic reactions is about the same. In Figure 3d, the first- and second-law efficiencies are shown. Based on Equation (16), the first-law efficiency depends on the H_2 and CO yields. Because of higher H_2 and CO yields at higher T_{in}, η_I increases with increased T_{in}. However, the variation in η_{II} is opposite that of η_I. Increased T_{in} implies that the chemical reaction is more complete towards the product side. Since the chemical reaction is a highly irreversible process, high exergy destruction due to the chemical reaction is expected. This results in decreased η_{II} as T_{in} increases. For the low T_{in} regime, exergy destruction due to the chemical reaction is low because of low catalytic activity. Moreover, the contributions of exergy destruction from compressors, pump, heaters and mixers are small. This leads to high η_{II} in the low T_{in} regime.
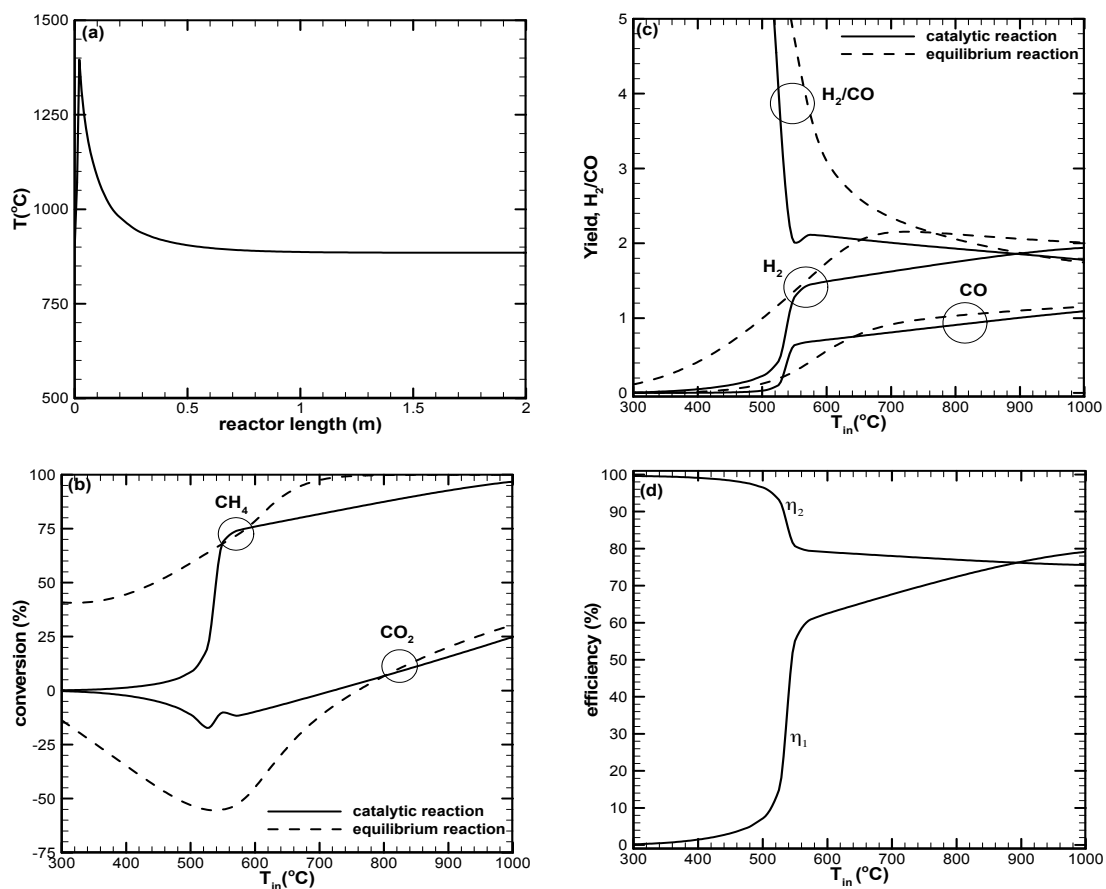
Figure 3. Performance of tri-reforming (TR) process obtained using the base operation conditions listed in Table 1. (**a**) Temperature variation along reactor with T_{in} = 900 °C; (**b**) CH_4 and CO_2 conversions; (**c**) H_2 yield, CO yield, and H_2/CO ratio; and (**d**) First- and second-law efficiencies.

In Figure 4, the variation of species mole fraction of the TR process using the base operation conditions listed in Table 1 is shown. It can be seen that significant mole fraction variation can be found when T_{in} is higher than 500 °C. The mole fractions of reactants (CH_4, CO_2, H_2O, O_2, and N_2) decrease while the mole fractions of products (CO and H_2) increase as T_{in} increases. Due to a highly active methane oxidation reaction, O_2 is consumed completely when T_{in} is greater than 550 °C. Also note that the variation trend of mole fractions of CO and H_2 are similar to the yields of CO and H_2 presented in Figure 3c. The yields of H_2 and CO are used to characterize the TR process performance in this study.
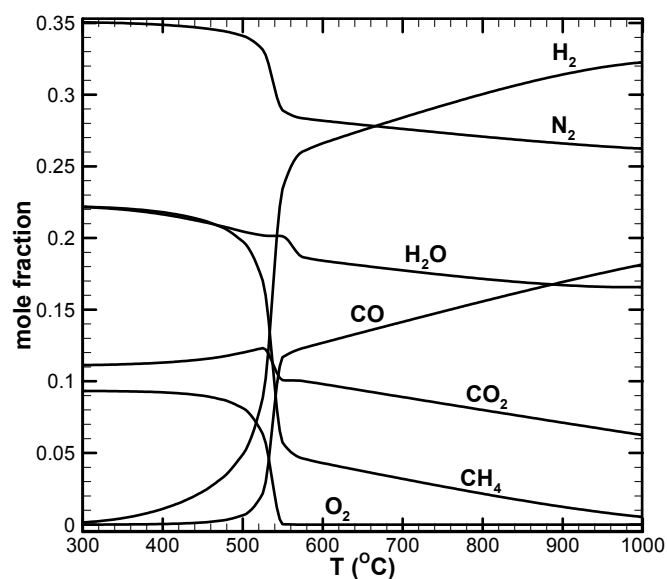
Figure 4. Variations of species mole fraction of the TR process using the base operation conditions listed in Table 1.

In the following, parametric studies based on the base operation conditions listed in Table 1 are carried out. As listed in Table 1, the inlet temperature of the reactant is the primary parameter and the amount of CH_4 fed is used as the reference for the species contained in the reactant and product. The catalyst weight (W) is varied from 0.025 g to 2.5 g; the operation pressure (P) is varied from 10 to 30 atm; the air/CH_4 ratio is varied from 1 to 3; H_2O/CH_4 is varied from 1 to 3; and CO_2/CH_4 is varied from 0.25 to 0.75.

In Figure 5 the effect of W/F ratios on the TR process is examined. The results shown in Figure 4 were obtained by varying the catalyst weight, while other parameters listed in Table 1 were kept fixed. That is, higher W/F ratio results when the catalyst weight is increased. As shown in Figure 5a, a higher temperature along the reactor length is obtained for the W/F = 0.00576 ghL^{-1} case. This indicates that a smaller amount of energy released from methane oxidation reaction is used for endothermic SR and DR reactions. For W/F = 0.0576 and 0.576 ghL^{-1} cases, temperature variations are identical at the reactor downstream. That is, there is a limiting W/F ratio for the reaction. Increasing the W/F ratio (either increasing catalyst weight or decreasing reactant volumetric flow rate) may not lead to further improved reaction performance. In Figure 5b, CH_4 and CO_2 conversions are shown. Due to low catalyst activity, CH_4 conversion is low when T_{in} is low. It can be seen that the T_{in} at which CH_4 conversion abruptly increases can be decreased by increasing the W/F ratio. That is, the catalyst activation temperature can be lowered with increased W/F ratio. As shown in Figure 5b, the T_{in} at which CH_4 conversion increases abruptly are 700 °C, 500 °C and 400 °C for W/F = 0.00576, 0.0576, and 0.576 gLh^{-1}, respectively. CH_4 conversions for the W/F = 0.0576 and 0.576 gLh^{-1} cases become identical when T_{in} is higher than 550 °C. As discussed above, limited performance results when the W/F ratio is increased. From Figure 5b, CO_2 conversion has a negative value except in the high T_{in} regime. This is due to CO_2 formation in the methane oxidation and WGS reactions while DR is less active. At high temperatures, CO_2 is consumed via the dry reforming reaction, leading to positive CO_2 conversion. In Figure 5c, the H_2/CO ratios for various W/F ratios are shown. It can be seen that H_2/CO ratio is about the same for the three W/F ratios studied when T_{in} is high. The H_2/CO ratio close to a value of 2 can be obtained for the W/F range studied. In Figure 5d, variations in η_I and η_{II} are shown. It can be seen that η_I can be enhanced by increasing the W/F ratio. However, η_{II} decreases when the W/F ratio is increased because of a more complete chemical reaction.
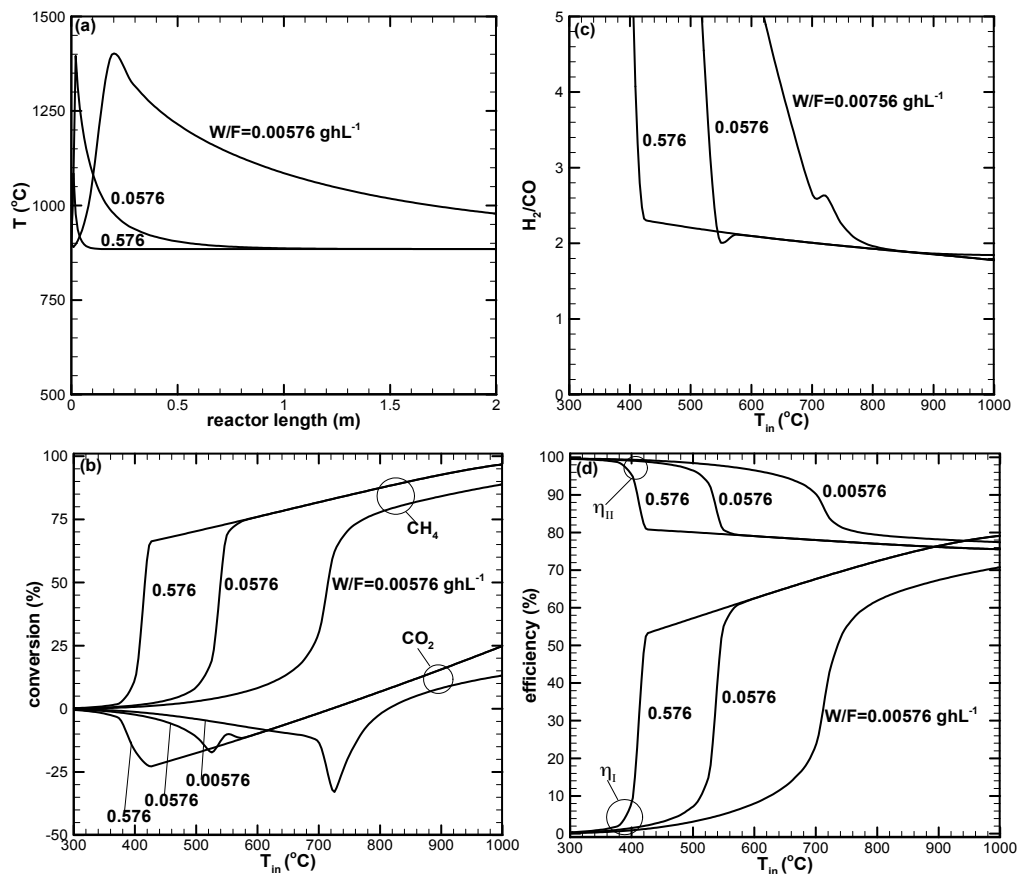
Figure 5. Effect of catalyst weight/volume flow rate (W/F) ratios on the TR process. Catalyst weight is varied from 0.025 to 2.5 g while the other parameters were kept unchanged, as listed in Table 1. (**a**) Temperature variation along reactor with T_{in} = 900 °C; (**b**) CH_4 and CO_2 conversions; (**c**) H_2/CO ratio; and (**d**) first- and second-law efficiencies.

In Figure 6, the reactor operating pressure effect on TR process performance is examined. From Figure 6a the highest temperature increases with increased operating pressure. As the high temperature in the near-entrance region of the reactor is due to the methane oxidation reaction, this implies that methane oxidation can be enhanced by increasing the operating pressure. Due to the enhanced methane oxidation reaction, the T_{in} at which an abrupt increase in CH_4 conversion occurs can be decreased by increasing the pressure, as shown in Figure 6b. Figure 6b also shows that CH_4 conversion can be increased in the low T_{in} regime when the pressure is increased. That is, increased operating pressure can enhance catalyst activity at lower temperatures. In the high T_{in} regime, CH_4 conversion is slightly decreased as the pressure is increased. Although higher CH_4 conversion can be obtained from lower pressure operations, the resulting syngas may not be suitable for further use because most applications involve high-pressure synthetic processes. A H_2/CO ratio with a value close to 2 is obtained for all the pressures studied when T_{in} is high, as shown in Figure 6c. Because of the reduced CH_4 conversion at a high T_{in} regime, it can be seen that η_I decreases with increased T_{in} and pressure, as shown in Figure 6d. However, Figure 6d shows that η_{II} increases with decreasing pressure because of less exergy destruction by the chemical reaction.
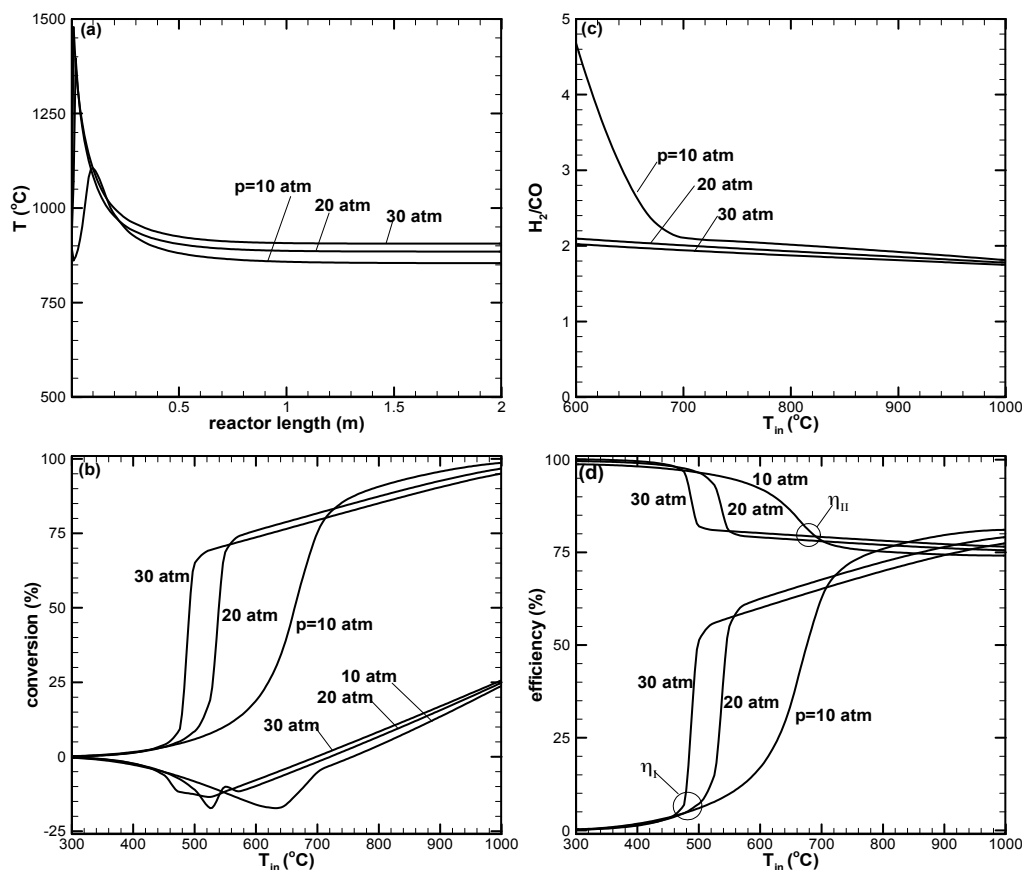
Figure 6. Effect of pressure on the TR process. Pressure is varied from 10 to 30 atm while the other parameters were kept unchanged, as listed in Table 1. (**a**) Temperature variation along reactor with $T_{in} = 900\ ^\circ$C; (**b**) CH_4 and CO_2 conversions; (**c**) H_2/CO ratio; and (**d**) first- and second-law efficiencies.

The variation in reactant composition effect on TR process performance is examined in the following. Figure 7 shows the air amount effect. Figure 7a shows that temperature can be increased using more air as the reactant. That is, a more complete methane oxidation reaction is achieved when the air supply is increased. With the increase in air amount, both CH_4 and CO_2 conversions can be enhanced, as shown in Figure 7b. For the Air/CH_4 = 3 case, 100% CH_4 conversion can be reached for T_{in} higher than 550 °C. Due to the increased energy supply, dry reforming can occur in the lower T_{in} regime resulting in increased CO_2 conversion. However, negative CO_2 conversion is still found when T_{in} is low. Although more N_2 is also introduced, increasing the volumetric flow rate of the entire reactant, it does not affect CH_4 and CO_2 conversions. As shown in Figure 7c, a H_2/CO ratio with a value higher than 2 can be obtained for the Air/CH_4 = 3 case because DR is more active when the temperature is high. For the Air/CH_4 = 1 case, the H_2/CO value is lower than 2. This is due to the reverse WGS reaction at high temperatures, reducing the H_2 amount. Because of decreased H_2 yield, lower η_I in the higher T_{in} regime is obtained, as shown in Figure 7d. The reverse WGS reaction also causes η_{II} to increase with T_{in} in the high T_{in} regime.
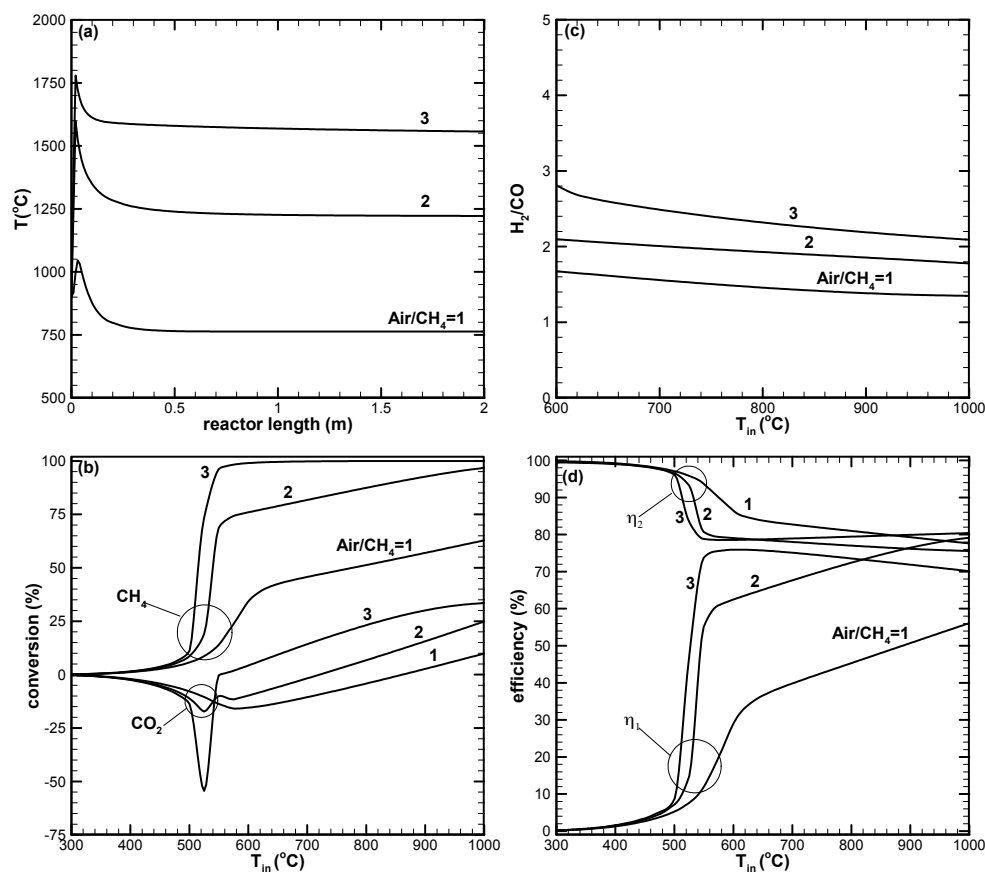
Figure 7. Air/CH$_4$ ratio effect on the TR process. The Air/CH$_4$ ratio is varied from 1 to 3 while the other parameters are kept unchanged, as listed in Table 1. (**a**) Temperature variation along the reactor with T_{in} = 900 °C; (**b**) CH$_4$ and CO$_2$ conversions; (**c**) H$_2$/CO ratio; and (**d**) first- and second-law efficiencies.

Figure 8 shows the H$_2$O amount effect on TR process performance. With increased H$_2$O in the reaction, lower temperature results at the reactor entrance region, as shown in Figure 8a, because of an increased reactant volumetric flow rate and endothermic SR reaction. The increased H$_2$O amount does not affect CH$_4$ conversion, as shown in Figure 8b. However, more negative CO$_2$ conversion results. In addition to CO$_2$ produced from methane oxidation, CO$_2$ may also be produced from WGS and RCM reactions, as indicated in Equations (4) and (5) when H$_2$O is increased. As shown in Figure 8c, a higher H$_2$/CO ratio is obtained when H$_2$O is increased because of increased H$_2$ yield. Figure 8d shows lower η_I results when the H$_2$O amount is increased. This is because higher heating to the reactant is required when the H$_2$O amount is increased. η_{II} increases with increased H$_2$O amount, indicating that less exergy destruction results as H$_2$O is increased.

Figure 9 shows the amount of CO$_2$ contained in the biogas effect on the TR process. As shown in Figure 9a, the amount of CO$_2$ does not affect the reaction temperature to a large extent. The temperature increases slightly as the CO$_2$ amount is decreased. As shown in Figure 9b, CH$_4$ conversion is affected insignificantly by the CO$_2$ amount. However, CO$_2$ conversion is always negative for the CO$_2$/CH$_4$ = 0.25 case. That is, more CO$_2$ is produced as a result of SR and WGS reactions than that consumed by DR and reverse WGS reactions. In Figure 9c, higher H$_2$/CO results when CO$_2$ is decreased. This may be due to less CO formed from CO$_2$ conversion. As with CH$_4$ conversion, the CO$_2$ amount effect on first- and second-law efficiencies is not significant, as shown in Figure 9d.
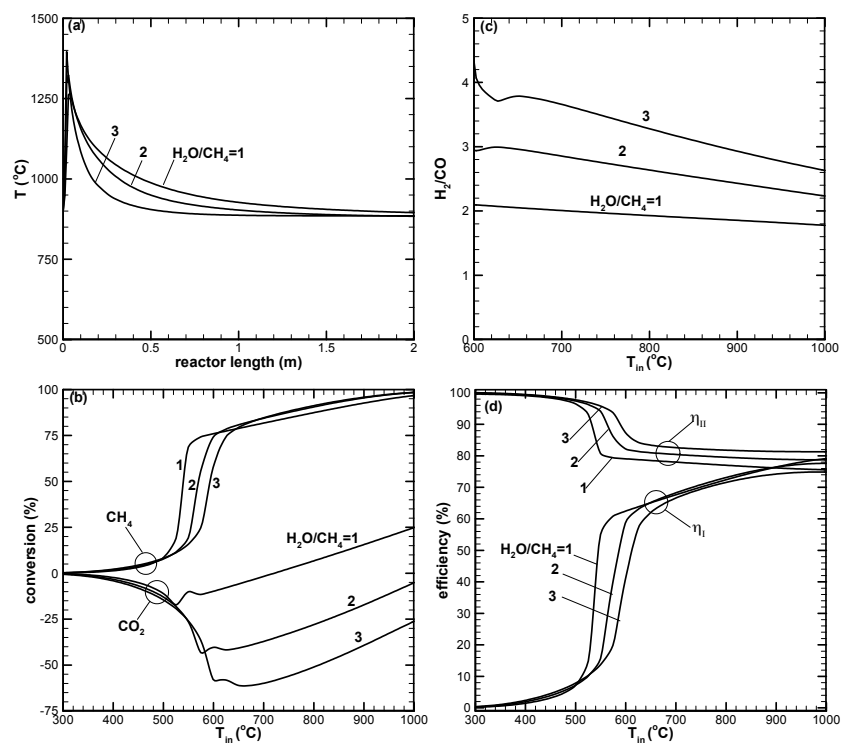
Figure 8. Effect of H_2O/CH_4 ratios on the TR process. H_2O/CH_4 is varied from 1 to 3 while the other parameters were kept unchanged, as listed in Table 1. (**a**) Temperature variation along reactor with T_{in} = 900 °C; (**b**) CH_4 and CO_2 conversions; (**c**) H_2/CO ratio; and (**d**) first- and second-law efficiencies.
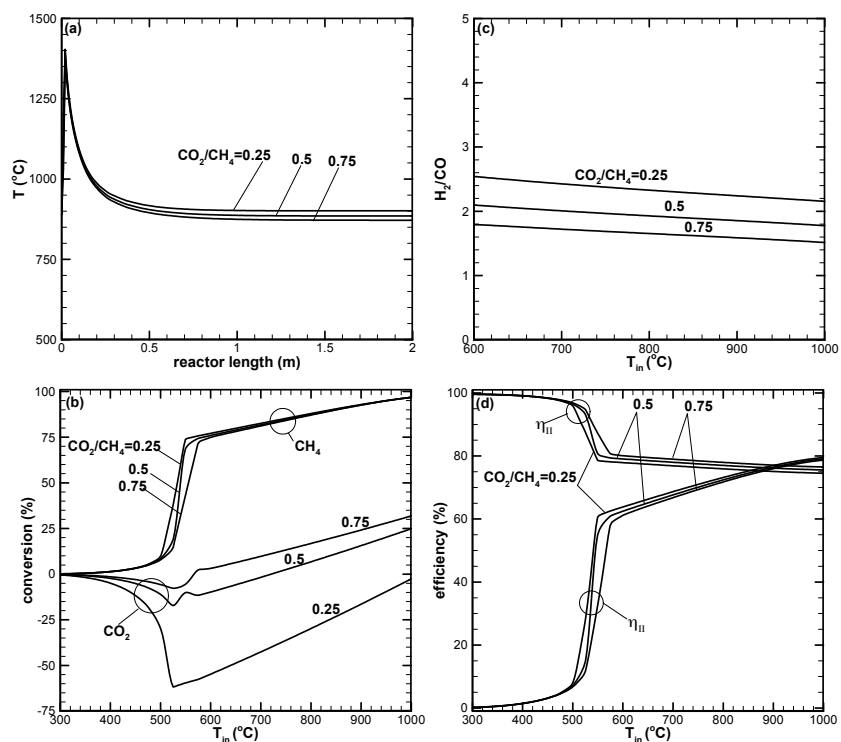
Figure 9. Effect of CO_2/CH_4 ratios on the TR process. CO_2/CH_4 is varied from 0.25 to 0.75 while the other parameters were kept unchanged, as listed in Table 1. (**a**) Temperature variation along reactor with T_{in} = 900 °C; (**b**) CH_4 and CO_2 conversions; (**c**) H_2/CO ratio; and (**d**) first- and second-law efficiencies.

Typical H_2 and CO yield results are shown in Figure 10 for various air and H_2O amounts. In Figure 10a, the H_2 and CO yields increase with the increased air added in the reactant. As a high temperature results in the $Air/CH_4 = 3$ case, the H_2 yield decreases with increased T_{in} due to the reverse WGS reaction. Figure 10b shows that H_2 yield can be enhanced by increased H_2O addition. CO yield also decreases with H_2O addition because of inactive DR and reverse WGS reactions. As a result, a higher H_2/CO ratio is obtained, as shown in Figure 8b.
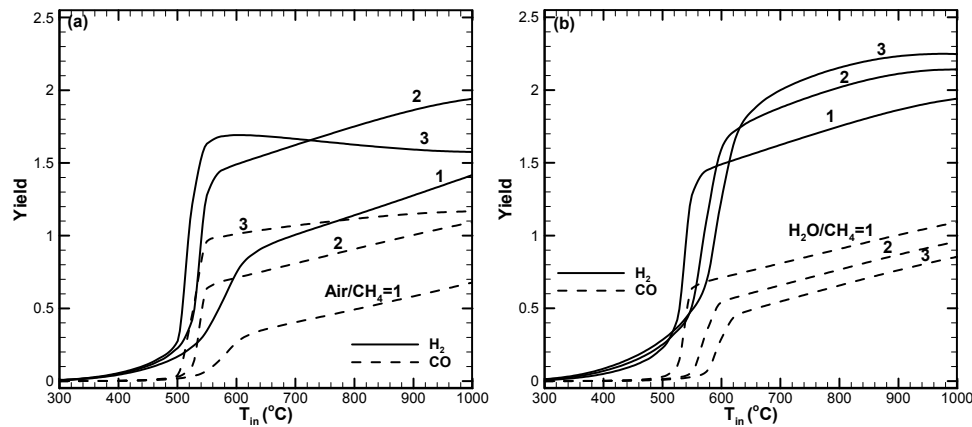
Figure 10. H_2 and CO yields for various (**a**) air and (**b**) H_2O amounts added.

From the results shown above, the CO_2 conversion is low or negative (CO_2 production). Positive CO_2 conversion only occurs in the high T_{in} regime. It is, then, desirable to determine the way to enhance CO_2 conversion in the TR process. After several sets of numerical experiments, it was found that high CO_2 conversion can be obtained when H_2O is low. In this case, the TR process approaches the dry reforming of methane (DRM). Figure 11 shows TR process performance with $H_2O/CH_4 = 0.001$. As shown in Figure 11a, the temperature drop occurs in the region very near the entrance because DRM is a highly endothermic reaction. Large amounts of required heat leads to this temperature drop. When the methane oxidation becomes active, energy release causes a temperature increase in the reactor downstream. In Figure 11b, CH_4 and CO_2 conversions are shown for the $H_2O/CH_4 = 0.001$ case. CO_2 conversion is always positive and increases with increased T_{in}. The CO_2 conversion is lower than that of CH_4 because of a low CO_2/CH_4 ratio in the biogas. Because of small amounts of H_2O, the H_2/CO ratio is close to unity, which is the stoichiometric H_2/CO ratio of DRM, as shown in Figure 11c. Figure 11d shows that η_I increases with increased T_{in} because of higher H_2 and CO yield. The second-law efficiency states that η_{II} decreases with increased T_{in} because of higher exergy destruction when the chemical reaction is more complete.
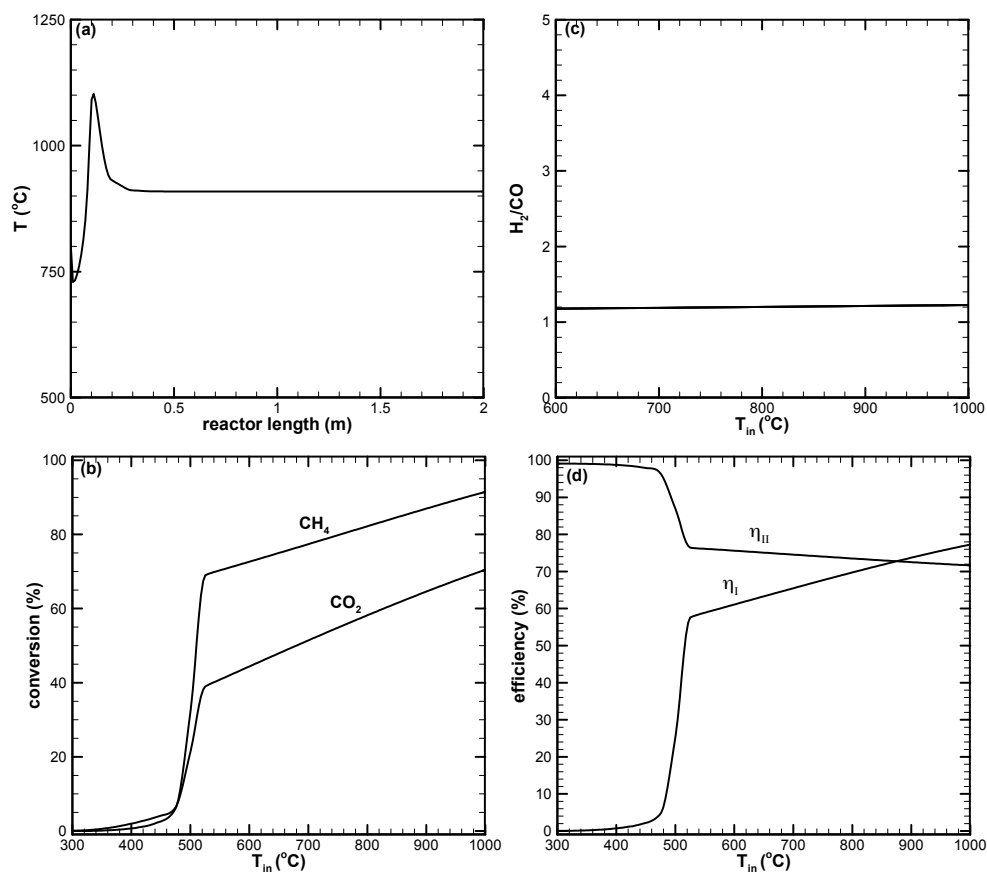
Figure 11. TR process with $H_2O/CH_4 = 0.001$ while the other parameters were kept unchanged, as listed in Table 1. (**a**) Temperature variation along reactor with T_{in} = 900 °C; (**b**) CH_4 and CO_2 conversions; (**c**) H_2/CO ratio; and (**d**) first- and second-law efficiencies.

4. Conclusions

The tri-reforming process was used in this study for syngas production from biogas. The effects of various operating parameters such as pressure, temperature and reactant composition were studied based on a model built in Aspen Plus. Based on the results obtained, the following conclusions can be drawn:

(1) There appears to be a limiting space velocity for the reaction. Beyond this limiting value, the reaction approaches the same performance. Lowering the reaction pressure could lead to higher CH_4 conversion, but the syngas produced may not be suitable for further applications.

(2) CH_4 and CO_2 conversions can be enhanced by increasing the amount of air in the reactant. Higher amounts of air could result in decreased H_2 yield due to the reverse water–gas shift reaction, which is favorable at high reaction temperatures.

(3) A higher H_2/CO ratio can be obtained by increasing H_2O addition. However, the dry reforming reaction is suppressed, leading to low CO_2 or negative conversion.

(4) Dry reforming of CO_2 can only be found when the reaction temperature is high. This results in positive CO_2 conversion and contributes to increased H_2 and CO yields.

(5) Higher CO_2 conversion can be obtained for the low H_2O addition case. However, low H_2/CO with a value close to unity results.

(6) The first-law efficiency increases with the increased reaction temperature because of higher H_2 and CO yields. The second-law efficiency decreases with the increased temperature because of higher exergy destruction due to a more complete chemical reaction at high temperatures.

Conflicts of Interest: The authors declare no conflict of interest.

Abbreviation

Nomenclature

d_p	catalyst particle diameter, m
Ex	exergy, kJ
e^{CH}	chemical exergy, kJ mol^{-1}
F	reactant volumetric flow rate, m^3 s^{-1}
K_j	surface adsorption equilibrium constant of species j, Pa^{-1}
K_j^C	surface adsorption equilibrium constant of species j in combustion reaction, Pa^{-1}
$K_{eq,i}$	equilibrium constant of reaction i
k_i	rate constant of reaction i, mol Pa$^{0.5}$kg$_{cat}$ s^{-1}, or mol Pa kg$_{cat}$ s^{-1}
L	length of reactor, m
LHV	lower heating value, kJ mol^{-1}
N_i	total molar flow rate of a stream i, mole s^{-1}
n_j	molar flow rate of species j, mole s^{-1}
p	pressure, Pa
Q	heat transfer, W
R	universal gas constant, 8.314 J mol^{-1} K^{-1}
R_b	reactor radius, m
r_i	kinetic rate of reaction i, mol kg$_{cat}$ s^{-1}
s	entropy, kJ mol^{-1} K^{-1}
T	temperature, K
W	catalyst weight, g
W_{comp}	compressor work, W
W_{pump}	pump work, W
X	species conversion
x	mole fraction
Y	species yield

Subscript

in	inlet
out	outlet
0	reference state

Greek symbols

ΔH	heat of reaction, kJ/mol
η	efficiency

References

1. Raju, A.S.K.; Park, C.S.; Norbeck, J.M. Synthesis gas production using steam hydrogasification and steam reforming. *Fuel Process. Technol.* **2009**, *90*, 330–336. [CrossRef]
2. Rathod, V.P.; Shete, J.; Bhale, P.V. Experimental investigation on biogas reforming to hydrogen rich syngas production using solar energy. *Int. J. Hydrog. Energy* **2016**, *41*, 132–138. [CrossRef]
3. Su, B.; Han, W.; Jin, H. Proposal and assessment of a novel integrated CCHP system with biogas steam reforming using solar energy. *Appl. Energy* **2017**, *206*, 1–11. [CrossRef]
4. Damanabi, A.T.; Bahadori, F. Improving GTL process by CO_2 utilization in tri-reforming reactor and application of membranes in Fischer-Tropsch reactor. *J. CO$_2$ Util.* **2017**, *21*, 227–237. [CrossRef]
5. Dwivedi, A.; Gudi, R.; Biswas, P. An improved tri-reforming based methanol production process for enhanced CO_2 valorization. *Int. J. Hydrog. Energy* **2017**, *42*, 23227–23241. [CrossRef]

6. Song, C.; Pan, W. Tri-reforming of methane: A novel concept for catalytic production of industrially useful synthesis gas with desired H_2/CO ratios. *Catal. Today* **2004**, *98*, 463–484. [CrossRef]

7. Majewski, A.J.; Wood, J. Tri-reforming of methane over $Ni@SiO_2$ catalyst. *Int. J. Hydrog. Energy* **2014**, *39*, 12578–12585. [CrossRef]

8. Kumar, N.; Shojaee, M.; Spivey, J.J. Catalytic bi-reforming of methane: From greenhouse gases to syngas. *Curr. Opin. Chem. Eng.* **2015**, *9*, 8–15. [CrossRef]

9. Choudhary, V.R.; Mondal, K.C.; Choudhary, T.V. Oxy-CO_2 reforming of methane to syngas over CoOx/MgO/SA-5205 catalyst. *Fuel* **2006**, *85*, 2484–2488. [CrossRef]

10. Weiland, P. Biogas production: Current state and perspectives. *Appl. Microbiol. Biotechnol.* **2010**, *85*, 849–860. [CrossRef] [PubMed]

11. Nicoletti, G.; Arcuri, N.; Nicoletti, G.; Bruno, R. A technical and environmental comparison between hydrogen and some fossil fuels. *Energy Convers. Manag.* **2015**, *89*, 205–213. [CrossRef]

12. Zhao, X.; Zhou, H.; Sikarwar, V.S.; Zhao, M.; Park, A.A.; Fennell, P.S.; Shen, L.; Fan, L. Biomass-based chemical looping technologies: The good, the bad and the future. *Energy Environ. Sci.* **2017**, *10*, 1885–1910. [CrossRef]

13. Samson, R.; LeDuy, A. Biogas production from anaerobic digestion of spirulina maxima algal biomass. *Biotechnol. Bioeng.* **2012**, *24*, 1919–1924. [CrossRef] [PubMed]

14. Rasi, S.; Veijanen, A.; Rintala, J. Trace compounds of biogas from different biogas production plants. *Energy* **2017**, *32*, 1370–1380. [CrossRef]

15. Hagman, L.; Blumenthal, A.; Eklund, M.; Svensson, N. The role of biogas solutions in sustainable biorefineries. *J. Clean. Prod.* **2018**, *172*, 3982–3989. [CrossRef]

16. Meyer, A.K.P.; Ehimen, E.A.; Holm-Nielsen, J.B. Future European biogas: Animal manure, straw and grass potentials for a sustainable European biogas production. *Biomass Bioenergy* **2018**, *111*, 154–164. [CrossRef]

17. Molino, A.; Larocca, V.; Chianese, S.; Musmarra, D. Biofuels production by biomass gasification: A review. *Energies* **2018**, *11*, 811. [CrossRef]

18. Chianese, S.; Loipersböck, J.; Malits, M.; Rauch, R.; Hofbauer, H.; Molino, A.; Musmarra, D. Hydrogen from the high temperature water gas shift reaction with an industrial Fe/Cr catalyst using biomass gasification tar rich synthesis gas. *Fuel Process. Technol.* **2015**, *132*, 39–48. [CrossRef]

19. Molino, A.; Migliori, M.; Blasi, A.; Davoli, M.; Marino, T.; Chianese, S.; Catizzone, E.; Giordano, G. Municipal waste leachate conversion via catalytic supercritical water gasification process. *Fuel* **2017**, *206*, 155–161. [CrossRef]

20. Chianese, S.; Fail, S.; Binder, M.; Rauch, R.; Hofbauer, H.; Molino, A.; Blasi, A.; Musmarra, D. Experimental investigations of hydrogen production from CO catalytic conversion of tar rich syngas by biomass gasification. *Catal. Today* **2016**, *277*, 182–191. [CrossRef]

21. Vita, A.; Pino, L.; Cipitì, F.; Laganà, M.; Recupero, V. Biogas as renewable rawmaterial for syngas production by tri-reforming process over $NiCeO_2$ catalysts: Optimal operative condition and effect of nickel content. *Fuel Process. Technol.* **2014**, *127*, 47–58. [CrossRef]

22. Lau, C.S.; Tsolakis, A.; Wyszynski, M.L. Biogas upgrade to syn-gas (H_2-CO) via dry and oxidative reforming. *Int. J. Hydrog. Energy* **2011**, *36*, 397–404. [CrossRef]

23. Zhu, X.; Li, K.; Liu, J.; Li, X.; Zhu, A. Effect of CO_2/CH_4 ratio on biogas reforming with added O_2 through an unique spark-shade plasma. *Int. J. Hydrog. Energy* **2014**, *39*, 13902–13908. [CrossRef]

24. Corigliano, O.; Fragiacomo, P. Technical analysis of hydrogen-rich stream generation through CO_2 reforming of biogas by using numerical modeling. *Fuel* **2015**, *158*, 538–548. [CrossRef]

25. Hernández, B.; Martín, M. Optimal process operation for biogas reforming to methanol: Effects of dry reforming and biogas composition. *Ind. Eng. Chem. Res.* **2016**, *55*, 6677–6685. [CrossRef]

26. Hajjaji, N.; Martinez, S.; Trably, E.; Steyer, J.; Helias, A. Life cycle assessment of hydrogen production from biogas reforming. *Int. J. Hydrog. Energy* **2016**, *41*, 6064–6075. [CrossRef]

27. Zhang, Y.; Zhang, S.; Benson, T. A conceptual design by integrating dimethyl ether (DME) production with tri-reforming process for CO_2 emission reduction. *Fuel Process. Technol.* **2015**, *131*, 7–13. [CrossRef]

28. Solovev, S.A.; Kurilets, Y.; Orlik, S.N. Tri-reforming of methane on structured Ni-containing catalysts. *Theor. Exp. Chem.* **2012**, *48*, 199–205. [CrossRef]

29. Cho, W.; Song, T.; Mitso, A.; McKinnon, T.J.; Ko, G.H.; Tolsma, J.E. Optimal design and operation of a natural gas tri-reforming reactor for DME synthesis. *Catal. Today* **2009**, *139*, 261–267. [CrossRef]

30. York, A.P.E.; Xiao, T.; Green, M.L.H. Brief overview of the partial oxidation of methane to synthesis gas. *Top. Catal.* **2003**, *22*, 345–358. [CrossRef]

31. Horn, R.; Williams, K.A.; Degenstein, N.J.; Bitsch-Larsen, A.; Dalle Nogare, D.; Tupy, S.A.; Schmidt, L.D. Methane catalytic partial oxidation on autothermal Rh and Pt foam catalysts: Oxidation and reforming zones, transport effects, and approach to thermodynamic equilibrium. *J. Catal.* **2007**, *249*, 380–393. [CrossRef]

32. De Groote, A.M.; Froment, D. Simulation of the catalytic partial oxidation of methane to syngas. *Appl. Catal. A* **1996**, *138*, 245–264. [CrossRef]

33. Scognamiglio, D.; Russo, L.; Maffettone, P.L.; Salemme, L.; Simeone, M.; Crescitelli, S. Modeling temperature profiles of a catalytic autothermal methane reformer with nickel catalyst. *Ind. Eng. Chem. Res.* **2009**, *48*, 1804–1815. [CrossRef]

34. Chan, S.H.; Wang, M.H. Thermodynamic analysis of natural gas fuel processing for fuel cell applications. *Int. J. Hydrog. Energy* **2000**, *25*, 441–449. [CrossRef]

35. Izquierdo, U.; García-García, I.; Gutierrez, Á.M.; Arraibi, J.R.; Barrio, V.L.; Cambra, J.F.; Arias, P.L. Catalyst deactivation and regeneration processes in biogas tri-reforming process. The effect of hydrogen sulfide addition. *Catalysts* **2018**, *8*, 12. [CrossRef]

36. Xu, J.; Froment, G.F. Methane steam reforming, methanation and water-gas shift: I. Intrinsic kinetics. *AIChE J.* **1989**, *35*, 88–96. [CrossRef]

37. Trimm, D.L.; Lam, C.W. The combustion of methane on platinum-alumina fibre catalysts. I. Kinetics and mechanism. *Chem. Eng. Sci.* **1908**, *35*, 1405–1413. [CrossRef]

38. De Smet, C.R.H.; de Croon, M.H.J.M.; Berger, R.J.; Marin, G.B.; Schouten, J.C. Design of adiabatic fixed-bed reactors for the partial oxidation of methane to synthesis gas. *Chem. Eng. Sci.* **2001**, *56*, 4849–4861. [CrossRef]

39. Bartholomew, C.H. Mechanisms of catalyst deactivation. *Appl. Catal. A Gen.* **2001**, *212*, 17–60. [CrossRef]

40. Velasco, J.A.; Fernandez, C.; Lopez, L.; Cabrera, S.; Boutonnet, M.; Jaras, S. Catalytic partial oxidation of methane over nickel and ruthenium based catalysts under low O_2/CH_4 ratios and with addition of steam. *Fuel* **2015**, *153*, 192–201. [CrossRef]

41. Ahmed, S.; Lee, S.H.E.; Ferrandon, M.S. Catalytic steam reforming of biogas e Effects of feed composition and operating conditions. *Int. J. Hydrog. Energy* **2015**, *40*, 1005–1015. [CrossRef]

42. Barbieri, G.; Di Maio, F.P. Simulation of the methane steam re-forming process in a catalytic Pd-membrane reactor. *Ind. Eng. Chem. Res.* **1997**, *36*, 2121–2127. [CrossRef]

43. Kim, J.H.; Choi, B.H.; Yi, J. Modified simulation of methane steam reforming in Pd-membrane/pack-bed type reactor. *J. Chem. Eng. Jpn.* **1999**, *32*, 760–769. [CrossRef]

44. Lutz, A.E.; Bradshaw, R.W.; Keller, J.O.; Witmer, D.E. Thermodynamic analysis of hydrogen production by steam reforming. *Int. J. Hydrog. Energy* **2003**, *28*, 159–167. [CrossRef]

45. Simpson, A.P.; Lutz, A.E. Exergy analysis of hydrogen production via steam methane reforming. *Int. J. Hydrog. Energy* **2007**, *32*, 4811–4820. [CrossRef]

46. Chein, R.; Wang, C.; Yu, C. Parametric study on catalytic tri-reforming of methane for syngas production. *Energy* **2017**, *118*, 1–17. [CrossRef]

47. Arab Aboosadi, Z.; Jahanmiri, A.H.; Rahimpour, M.R. Optimization of tri-reformer reactor to produce synthesis gas for methanol production using differential evolution (DE) method. *Appl. Energy* **2011**, *88*, 2691–2701. [CrossRef]